

pubs.acs.org/acscatalysis Research Article

Partial Oxidation of Methane Enabled by Decatungstate Photocatalysis Coupled to Free Radical Chemistry

Charles B. Musgrave III, Kaeleigh Olsen, Nichole S. Liebov, John T. Groves, William A. Goddard III, and T. Brent Gunnoe



Cite This: ACS Catal. 2023, 13, 6382-6395



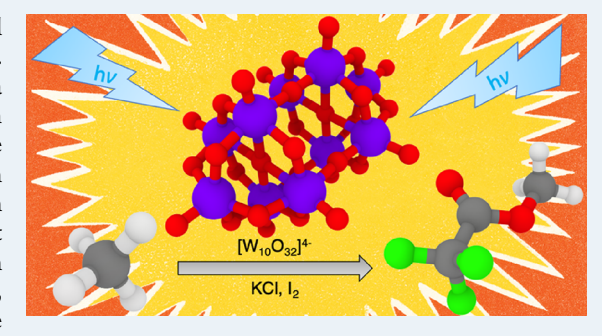
ACCESS I

III Metrics & More

Article Recommendations

s Supporting Information

ABSTRACT: The decatungstate anion, $[W_{10}O_{32}]^{4-}$ or DT, is a useful photocatalyst for organic transformations involving C–H functionalization. Herein, we leverage the unique photoredox properties of DT to generate a chlorine radical from chloride ion for the photochemical partial oxidation of methane. Under optimized conditions, the DT–chloride–iodine ensemble achieves methane to methyl trifluoroacetate conversion with >350 photocatalyst turnovers at ~60% yield based on methane in trifluoroacetic acid solvent. Methyl trifluoroacetate exhibits excellent stability under reaction conditions with minimal amounts of degradation (<6%) detected after 41 h. Based on density functional theory calculations, we propose a mechanism that involves synergistic relationships among the DT, chloride, and iodine species with the following key features: (1)



photoredox electron transfer reaction of DT with Cl⁻ to generate Cl•, (2) reaction of photoexcited DT with methane to generate methyl radicals via net hydrogen atom abstraction, (3) a Cl/I radical-based pathway in which methane is converted to MeTFA, and (4) reoxidation of reduced DT species by dioxygen. This mechanism takes advantage of the unique redox potential of DT and the ability of DT to mediate both electron transfer and hydrogen atom transfer reactions, ultimately generating an efficient pathway for aerobic methane partial oxidation.

KEYWORDS: methane partial oxidation, photocatalysis, C-H activation, hydrocarbon, decatungstate, DFT

INTRODUCTION

Conversion of light alkanes from natural gas into value-added chemicals is a cornerstone of the chemical industry. The development of new catalytic processes for the direct conversion of methane (and other light alkanes) to higher-value liquid products is important for the increased use of stranded natural gas and for other sources (e.g., biogas) of methane and light alkanes. Highly desired processes include the direct partial oxidation of methane, ethane, and propane to liquid products, so called direct gas-to-liquid (GTL) conversions, with a particular focus on methane-to-methanol. Given the substantial global natural gas reserves, which account for ~25% of global energy, there is enormous potential for direct GTL technologies. Additionally, these reserves are often in stranded locations, where at-wellhead GTL conversion is most desirable.

Current commercial methods for indirect methane-to-methanol conversion involve the highly energy- and capital-intensive methane-reforming reaction ($H_2O + CH_4 \rightarrow CO + 3$ H_2) followed by Fischer–Tropsch chemistry to produce methanol or longer chain hydrocarbons.^{5,6} A more desirable alternative is the direct mono-oxygenation of methane by O_2 to produce methanol. While methane partial oxidation using $\frac{1}{2}$ O_2

is thermodynamically favorable, challenges include (1) overcoming the large activation barrier required to break a nonpolar C–H bond of methane (bond dissociation energy $\approx 105~\rm kcal/mol)$ and (2) evading the over-oxidation of methanol due to the weaker C–H bond of methanol (96 kcal/mol) compared to methane. 7,8

Radical-based chemistry, such as catalytic oxychlorination, offers a route for C–H functionalization of light alkanes to produce functionalized products (eq 1). Unfortunately, such processes often suffer from the over-oxidation dilemma, again due to weaker C–H bonds in the product (e.g., $\sim\!100$ kcal/mol for CH₃Cl). In fact, methane conversion using catalytic oxychlorination is often limited to <10% in order to achieve adequately high selectivity.

$$CH_4 + HX + 1/2 O_2 \xrightarrow{\text{catalyst}} CH_3X + H_2O$$
 (1)

Received: February 16, 2023 Revised: March 29, 2023 Published: April 24, 2023





Electrophilic Pt(II) catalysis introduced by Shilov and coworkers was an early example of catalytic methane monofunctionalization, but this process suffered from the requirement of a stoichiometric Pt(IV) oxidant. 17 The Catalytica process pioneered by Periana and coworkers achieved methane-to-methyl bisulfate conversion with >70% yield and >90% selectivity using the key strategy of protecting the monofunctionalized product from over-oxidation by the electronwithdrawing bisulfate group. However, the energy requirements for the separation of product from oleum and reconcentration of sulfuric acid were a challenge for potential commercialization. ^{18,19} Molecular iodine has been shown to functionalize light alkanes in oleum, but this approach could not be extended to non-superacidic media. 20,21 Main group compounds, such as Tl(TFA)₃ and Pb(TFA)₄, and hypervalent iodine, namely, (C₆F₅)I^{III}(TFA)₂, have been shown to functionalize light alkanes in non-superacidic solvent, albeit stoichiometrically.²²

Metal-exchanged zeolites (e.g., copper) are capable of methane oxidation to methanol. However, these catalysts typically do not yield high methane conversion with high selectivity. Also, methanol extraction requires significant dilution for separation, which typically destroys the active site, requiring subsequent high-temperature oxidation for catalyst restoration. ³¹

To improve product yields, we and other groups have pursued a strategy to circumvent over-oxidation through the installation of a protecting group in the functionalized alkyl product.^{32,33} For example, we reported the thermal (100–235 $^{\circ}\mathrm{C})$ partial oxidation of light alkanes (methane, ethane, and propane) in trifluoroacetic acid (HTFA) by chloride-iodate and chloride-periodate systems via a method termed oxyesterification (OxE). OxE produced the corresponding alkyl esters (RTFA) with >20% yield relative to the alkanes and >80% selectivity toward mono-oxidized products. 34,35 We discovered that the ester moiety protects the products from subsequent oxidation, thus permitting the production of the corresponding alcohol, along with regeneration of HTFA through hydrolysis. 36,37 Oxygen-recyclable cobalt and manganese catalysts have also been shown to effectively oxidize methane in HTFA. $^{38-40}$ Recently, we reported the use of molecular Mn oxides and Mn salts for methane partial oxidation along with a mechanistic study.⁴

Several groups have reported photodriven C–H functionalization for which the generation of a chlorine radical from chloride appears to be a key step. Several examples of such reactions that are successful for unactivated hydrocarbons (e.g., cyclohexane) have been reported. $^{42-46}$ Using the strategy of generating chlorine from chloride, we recently pursued photodriven light alkane functionalization. 47,48 Higher yields were obtained for the chloride–iodate OxE process under photocatalytic conditions ($\sim\!50\%$ yield was achieved for methane) compared to yields for the analogous thermally driven reaction. We also reported that Fe(TFA)3 mediates photodriven hydrocarbon functionalization. The Similarly, FeCl3 has been shown to functionalize methane and heavier alkanes to a variety of products. The Schelter and Goldberg groups recently reported photodriven, aerobic alkane iodination in acetonitrile using catalytic ["Bu4N]Cl. The Schelter and Goldberg groups recently reported photodriven, aerobic alkane iodination in acetonitrile using catalytic ["Bu4N]Cl. The Schelter and Goldberg groups recently reported photodriven, aerobic alkane iodination in acetonitrile using catalytic ["Bu4N]Cl. The Schelter and Goldberg groups recently reported photodriven, aerobic alkane iodination in acetonitrile using catalytic ["Bu4N]Cl. The Schelter and Goldberg groups recently reported photodriven, aerobic alkane iodination in acetonitrile using catalytic ["Bu4N]Cl. The Schelter and Goldberg groups recently reported photodriven, aerobic alkane iodination in acetonitrile using catalytic ["Bu4N]Cl. The Schelter and Goldberg groups recently reported photodriven, aerobic alkane iodination in acetonitrile using catalytic ["Bu4N]Cl. The Schelter and Goldberg groups recently reported photodriven, aerobic alkane iodination in acetonitrile using catalytic ["Bu4N]Cl. The Schelter and Goldberg groups recently reported photodriven, aerobic alkane iodination in acetonitrile using catalytic ["Bu4N]Cl. The Schelter and Goldberg groups recentl

Polyoxometalates (POMs) have emerged as a widely successful class of photocatalysts for organic transformations due to their ability to perform both electron transfer (ET) and hydrogen atom transfer (HAT) reactions. ^{51–58} The decatung-

state anion ([W₁₀O₃₂]⁴⁻ or DT) is currently employed as a HAT photocatalyst because of its ready availability and the array of C–H bonds it can cleave. Furthermore, DT has been used for a variety of C(sp³)–H functionalizations, including C–C bond formations and oxidation reactions. Laudadio and coworkers reported the functionalization of light alkanes (e.g., methane, ethane, propane, and isobutane) to C–C coupled products using DT in a photocatalytic flow system. In a separate report, Laudadio and coworkers reported DT-mediated selective oxidation of aliphatic substrates to ketone-containing products. Figure 1 depicts the

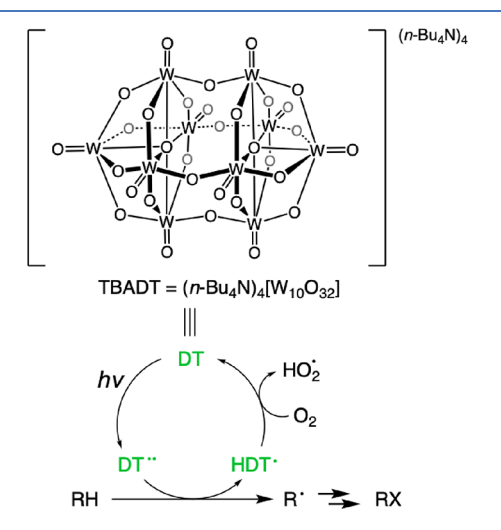


Figure 1. Simplified scheme showing capability of photoexcited decatungstate (DT $\bullet\bullet$) for hydrogen atom abstraction from a generic alkane (RH). HDT \bullet denotes the reduced radical species following hydrogen atom abstraction.

structure of the DT salt, TBADT [TBA = $(^nBu_4N)_4$], and its ability to perform HAT in its photoexcited state; here, DT $\bullet \bullet$ denotes the suspected excited triplet state (referred to in previous publications as wO or DT*) 76 and HDT \bullet denotes the reduced species after HAT.

Because our previously reported thermal and photoinitiated OxE processes for light alkane functionalization are proposed to rely on HAT, ^{36,37,48} we hypothesized that the addition of DT as a photodriven HAT reagent may accelerate the mono-oxidation of light alkanes to alkyl esters in a chloride—iodine system.

Of particular interest was the possibility that photoexcited DT could also generate chlorine atoms, Clo, under these reaction conditions due to the very high reduction potential of DT••. 62 There have been a number of recent advances in the photogeneration of Clo, including photoreduction of metal chlorides 43,44,46,47,80-83 and photoredox oxidation of chloride ion (Cl⁻). 42,84-86 As noted above, the generation of chlorine has been used to functionalize unactivated hydrocarbons. 42-46,87 DT is robust under acidic conditions and has a high quantum yield for photoexcitation, but it has not been employed for the generation of Clo as a C-H activation mediator. Herein, we report experimentally and validate computationally the use of DT as a photocatalyst for methane partial oxidation in the presence of chloride and iodine to form methyl trifluoroacetate (MeTFA) and methyl chloride (MeCl or CH₃Cl). In our best case, this DT-chloride-iodine aerobic process achieved methane to MeTFA conversion with >350

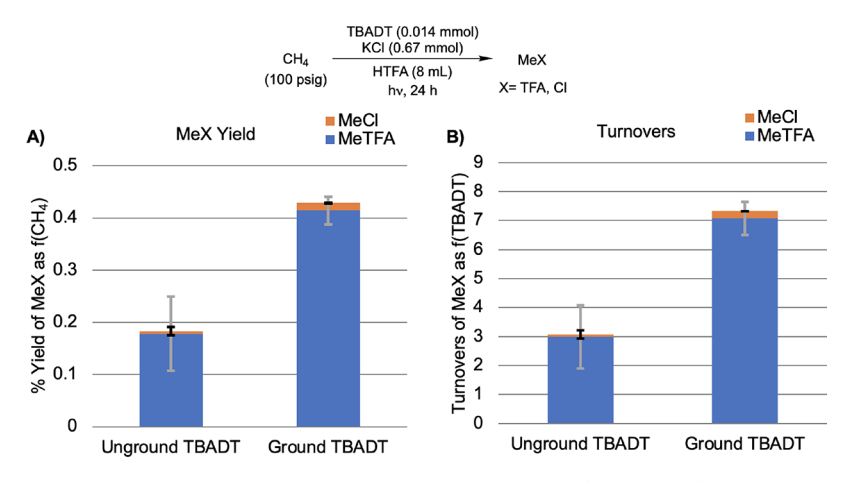


Figure 2. Initial screening for the photochemical functionalization of methane by TBADT (0.014 mmol) and KCl (0.67 mmol) in HTFA after 24 h of mercury arc lamp irradiation. TBADT was either used directly or ground before addition to the reactor. MeX (X = TFA, Cl) is plotted as methane conversion (A) and catalytic turnovers based on TBADT (B). Each bar graph represents the average of a minimum of three independent experiments with error bars depicting the standard deviation of the three experiments.

photocatalyst turnovers (TOs) and ~60% yield based on methane.

RESULTS AND DISCUSSION

Reagent Screening and Optimization. An initial screening of the photochemical reactivity of an aerobic mixture of TBADT (0.014 mmol) and KCl (0.67 mmol) in HTFA (8 mL) pressurized with 100 psig of methane (~24 mmol) resulted in the formation of 0.043 ± 0.015 mmol of MeX (X = TFA, Cl) after 24 h of mercury arc lamp irradiation. This corresponds to a yield of 0.18 \pm 0.071% and a 42:1 ratio of MeTFA to MeCl. Herein, percent yields are reported with respect to methane, and all data are the result of a minimum of three separate experiments with standard deviations. Product formation was determined by ¹H NMR spectroscopy and referenced against a known amount of either HOAc or CH₃NO₂ as an internal standard. When TBADT was ground using a mortar and pestle before addition to the reactor (with all other conditions unchanged), 0.10 ± 0.008 mmol of MeX was produced in $0.43 \pm 0.027\%$ yield with a 33:1 ratio of MeTFA to MeCl (Figure 2). The corresponding TOs of TBADT were 3.1 \pm 1.1 and 7.3 \pm 0.58 when TBADT was unground and ground, respectively. The increased product formation and the decreased standard deviation using the ground TBADT suggest that the smaller particle size increased TBADT's solubility in HTFA. Under reaction conditions, the TBADT is not fully soluble, which provides a likely explanation for the observed effect of grinding the TBADT.

The analogous reaction to that shown in Figure 1 but in the absence of KCl produced no MeTFA; this is likely because no radical traps are present to quench CH₃● (see below for mechanism discussion). Various loadings of KCl were tested, and it was observed that doubling the KCl loading from 0.67 mmol to 1.34 mmol had a positive effect on the MeX yield; however, increasing the KCl loading to 2.68 mmol had minimal effect, within deviation, on the MeX yield (Figure 3A). Using 1.34 mmol of KCl, various loadings of TBADT were tested, with the optimal amount of TBADT being 0.007 mmol as this maximized the MeX yield (Figure 3B).

In our previous reports of light alkane partial oxidation using iodate as the oxidant, mechanistic studies indicated that I_2 is likely generated in situ from iodate and serves to trap alkyl

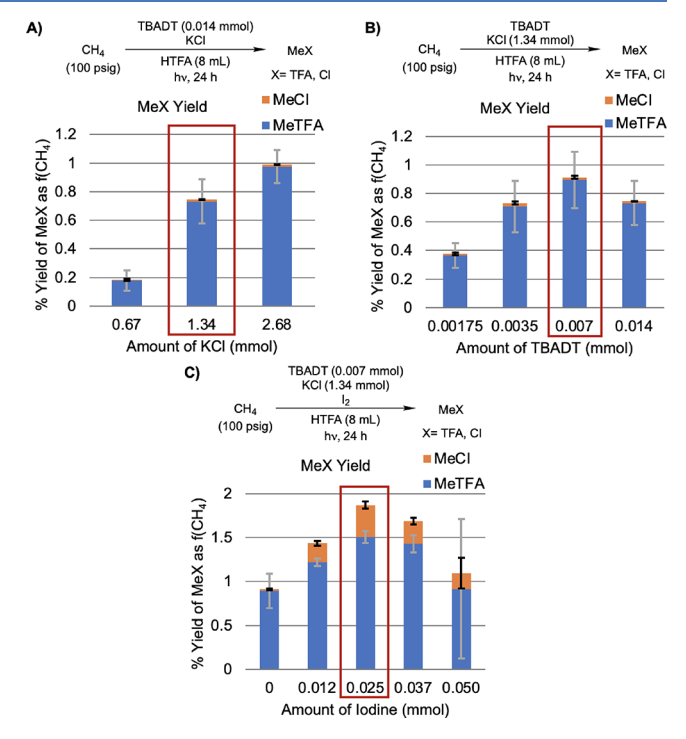


Figure 3. MeX (X = TFA, Cl) yield at various loadings of KCl (A), TBADT (B), and I_2 (C). Red boxes indicate optimal reagent loadings in standard aerobic reaction conditions. Each bar graph represents the average of at least three independent experiments with error bars depicting the standard deviations.

radicals in solution.³⁶ Thus, I_2 was explored as a reaction additive in our TBADT photochemistry. We found 0.025 mmol of I_2 to be optimal as this loading maximized the MeX yield (Figure 3C). The addition of TBADT, KCl, and I_2 in their optimized loadings in 8 mL of HTFA led to the formation of 0.45 \pm 0.030 mmol of MeX in 1.9 \pm 0.078% yield with a 4.2:1 ratio of MeTFA to MeCl after 24 h of mercury arc lamp irradiation. This MeX formation as a function of TBADT corresponds to 64 \pm 4.3 TOs. These optimized reagent loadings in 8 mL of HTFA and 100 psig of CH₄ will be referred to as the standard aerobic reaction conditions throughout the remainder of this contribution.

Other combinations of TBADT, KCl, and/or I_2 in HTFA led to decreased CH_4 functionalization (Table 1). For the

Table 1. MeX (X = TFA, Cl) Yields for the Control Reactions of Remaining Combinations of Reagents^a

entry	reagents	% yield of MeTFA	% yield of MeCl
1	TBADT (0.007 mmol), I ₂ (0.025 mmol)	0.13 ± 0.069	0
2	KCl (1.34 mmol)	0.36 ± 0.069	0.010 ± 0.0088
3	I ₂ (0.025 mmol)	0.50 ± 0.16	0
4	KCl (1.34 mmol), I ₂ (0.050 mmol)	0.010 ± 0.010	0
5	KCl (1.34 mmol), I ₂ (0.025 mmol)	1.7 ± 0.26	0.42 ± 0.063

^aThe reagents were added to 8 mL of HTFA, pressurized with 100 psig of CH₄, and irradiated with a mercury arc lamp for 24 h. Each entry line represents the average of at least three independent experiments reported with their standard deviations.

reaction of KCl and I2, it was found that iodine loading is crucial for MeX production. Specifically, increasing the loading of I₂ to 0.050 mmol with 1.34 mmol of KCl led to no MeX production within standard deviation (Table 1, entry 4). However, halving the amount of I₂ to 0.025 mmol with 1.34 of mmol KCl (corresponding to standard aerobic reaction conditions) led to substantial MeX formation (Table 1, entry 5). The investigation of the background reaction of 1.34 mmol of KCl and 0.025 mmol of I2 for methane functionalization in HTFA is described in the Supporting Information. The bimodal nature of MeX production as a function of time for this background reaction can be seen in Figure S5. The bifurcated results hint that radical chain processes for MeX formation are possible, but the initiation of such reactions is highly dependent on factors that we could not identify nor control.

Additional control reactions were performed. When heated (180 $^{\circ}$ C for 3 h) without irradiation, TBADT (0.014 mmol) and KCl (1.34 mmol) in HTFA (8 mL) with 100 psig of CH₄ resulted in no MeX formation. When the standard aerobic reaction conditions were pressurized with 100 psig of Ar instead of CH₄ and subjected to a mercury arc lamp for 24 h, MeX production was not observed. Minimal methane

functionalization (<0.03% yield) occurred when KBr was used in place of KCl under the standard aerobic reaction conditions. When the standard aerobic reaction conditions were instead subjected to fume hood LED lighting or a 370 nm LED lamp, CH₄ functionalization occurred, albeit at much slower rates and with lower yields. Acetic acid (HOAc) was explored as a solvent alternative to HTFA. With pure HOAc as solvent, MeX formation was not observed. Using HOAc and HTFA solvent mixtures, the chemistry was not clean enough to extract meaningful results.

Using standard aerobic reaction conditions, CH₄ pressure was varied (Figure 4). At lower methane pressures, MeX yield based on methane was improved in the TBADT–KCl–I₂ system. For example, reacting TBADT (0.007 mmol), KCl (1.34 mmol), and I₂ (0.025 mmol) with 15 psig of methane (~4 mmol) afforded 0.35 \pm 0.0057 mmol of MeX in 8.9 \pm 0.58% yield with a 6.4:1 ratio of MeTFA to MeCl after 24 h of reaction. This MeX formation corresponds to 50 \pm 0.82 TOs of TBADT. This is the highest conversion achieved with this system under aerobic conditions (i.e., without the inclusion of additional dioxygen).

MeTFA Stability, Kinetics of Methane Functionalization, and Photocatalyst Reoxidation with Dioxygen. Product stability was explored under standard aerobic reaction conditions with the addition of 0.35 mmol of MeTFA at time t = 0 h and pressurization with 100 psig of Ar in place of CH₄. MeTFA was found to be stable under these conditions with >94% MeTFA remaining after 41 h (Figure 5).

Using standard aerobic reaction conditions, the time of mercury arc lamp irradiation was varied to explore CH₄ oxidation as a function of time (Figure 5). According to product formation versus time, it appears that MeX formation halts at $t \cong 21$ h. However, the exact time is difficult to discern due to the large deviations inherent to the photoreactions. The lack of further product formation after $t \cong 21$ h could indicate depletion of the limiting reagent. At t = 21 h, 0.44 \pm 0.010 mmol of MeX was present. This corresponds to 62 \pm 1.5 TOs of TBADT and consumption of \sim 32% of starting KCl.

Using the standard aerobic reaction conditions, the reagents were added to the reactor in air and then sealed. It was speculated that the dioxygen present in the headspace of the reactor was fully consumed at $t\cong 21$ h, thus preventing photocatalyst reoxidation. The amount of dioxygen estimated

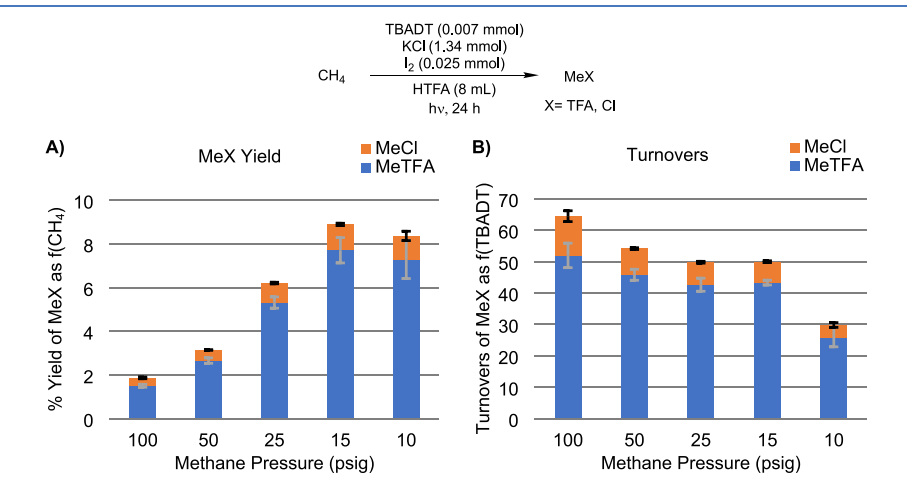


Figure 4. Effect of methane pressure on MeX (X = TFA, Cl) yield (A) and the corresponding catalyst TOs (B). Each bar graph represents the average of at least three independent experiments with error bars depicting the standard deviations.

ACS Catalysis pubs.acs.org/acscatalysis Research Article

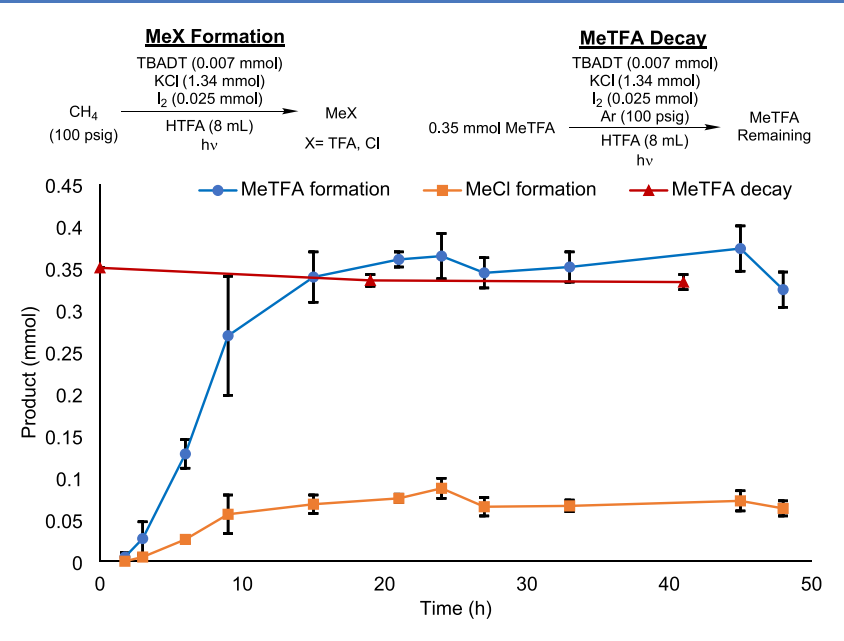


Figure 5. Methane functionalization and MeTFA decay under standard aerobic reaction conditions with TBADT, KCl, and I_2 as a function of time. Each data point represents the average of at least three independent experiments with error bars depicting the standard deviations.

Scheme 1. Effect of Differing Concentrations of Dioxygen on MeX (X = TFA, Cl) Production Reported as mmol of Product, Catalyst Turnovers, and Percent Yield^a

"A = standard aerobic reaction conditions; B = dinitrogen-purged reaction solution; C = dioxygen-purged reaction solution. Each reaction scheme represents the average of at least three independent experiments reported with their standard deviation.

to be in the headspace was calculated to be \sim 0.75 mmol. Thus, at $t \cong 21$ h, the concentration of dioxygen likely becomes too low to reoxidize TBADT. This speculation is further supported by the blue color of the post-reaction solutions, indicative of spent decatungstate in its reduced form.

We began our studies on dioxygen dependence by varying the amount of dioxygen present in the reactor headspace before the start of the reaction. It has been shown that dioxygen is incapable of quenching DT $\bullet \bullet$ such that catalyst deactivation by dioxygen is very unlikely. We studied the impact of dioxygen by purging the reaction solution with either dinitrogen or dioxygen. Purging was performed by bubbling the respective gas into the reaction solution for 1 min after charging the reactor with TBADT, KCl, I₂, and HTFA and before pressurizing with CH₄. When the solution was purged with dinitrogen, no MeX was produced (Scheme 1B). When the solution was purged with dioxygen, 0.90 \pm 0.30 mmol of MeX was produced after 24 h of irradiation (Scheme 1C).

Scheme 1 details a comparison of these solution-purged reactions to the standard aerobic reaction. These results provide support for dioxygen as the limiting reagent in which dioxygen reoxidizes spent TBADT back to its active form.

Additional experiments were performed to further probe the reoxidation of TBADT by dioxygen. After irradiation of the high methane conversion aerobic reaction conditions (15 psig of CH₄) for 24 h, dioxygen top pressure was added to the reactors followed by further irradiation. A series of experiments were performed in which we modulated the amount of dioxygen added, the number of dioxygen pressurizations, and the amount of irradiation time between dioxygen top pressure additions. In many of these experiments, the formation of MeCl could not be accurately quantified due to signal broadening in the ¹H NMR spectra (see Figure S3 for the representative ¹H NMR spectrum). A preliminary reoxidation reaction as well as the optimal reoxidation reaction are displayed in Scheme 2, along with the high-methane

Scheme 2. Comparison of High-Yield Aerobic Methane Oxidation to MeX (X = TFA, Cl) Reaction with Standard Reagent Loadings (A) to Preliminary Reoxidation Reaction with Standard Reagent Loadings (B) and Optimal Reoxidation Reaction with Standard Reagent Loadings (C)⁴

A) High Yield Aerobic Reaction

TBADT (0.007 mmol) KCI (1.34 mmol)
$$\frac{1_2 (0.025 \text{ mmol})}{1_2 (0.025 \text{ mmol})}$$
 43 ± 0.76 TOs MeTFA + 6.7 ± 0.29 TOs MeCI 7.7 ± 0.58% yield MeTFA + 1.2 ± 0.054% yield MeCI hv. 24 h

B) Preliminary Re-oxidation Reaction

C) Optimal Re-oxidation Reaction

$$\begin{array}{c} \text{TBADT (0.007 mmol)} \\ \text{KCI (1.34 mmol)} \\ \text{I}_2 \text{ (0.025 mmol)} \\ \text{(20 psig)} \end{array} \\ \begin{array}{c} \text{HTFA (8 mL)} \\ \text{O}_2 \text{ purge} \\ \text{hv, 24 h} \end{array} \\ \text{x 6} \end{array} \\ \begin{array}{c} \text{370 \pm 85 TOs MeTFA} \\ \text{59 \pm 14\% yield MeTFA} \\ \text{*Cannot detect MeCl due to line broadening} \\ \text{*Cannot detect MeCl due to line broadening} \\ \end{array}$$

"Results are reported as catalyst TOs and percent yields based on methane. Each reaction scheme represents the average of at least three independent experiments reported with their standard deviation.

conversion aerobic reaction for comparison. We note that the optimal reoxidation experiment reached the pressure limitations of the reaction vessel. Because dioxygen is our limiting reagent under these conditions, it is feasible that MeX formation will continue with additional dioxygen if a reactor with a higher pressure limit or continuous flow of dioxygen is used.

In an effort to circumvent the pressure limitations of the reactors described above with dioxygen, non-gaseous additives were explored as potential co-oxidants, such as copper salts and peroxides. None of the copper salts explored (CuCl₂·xH₂O₃) $Cu(OAc)_2 \cdot xH_2O[OAc = C_2H_3O_2^{-1}]$, or $Cu(TFA)_2 \cdot xH_2O)$ nor K₂S₂O₈ had any beneficial effect on product formation (Figure S4). Alkyl peroxides (tert-butyl hydroperoxide and di-tert-butyl peroxide) were then explored as potential co-oxidants, resulting in >100% yield of MeX (Table S1). However, this >100% MeX yield was due to peroxide decomposition for which photoinduced cleavage of the peroxide O-O bond followed by decomposition leads to the production of methyl radicals and acetone (see the Supporting Information for details). 89,90 When hydrogen peroxide (which is unable to generate methyl radicals) was used, no improvement of MeX yield (within deviation) was observed relative to the high yield aerobic reaction. The large deviations for these reactions can be explained by photodecomposition. UV irradiation initiates O-O bond cleavage to hydroxyl radicals, which form water and dioxygen through a radical chain mechanism, leading to differing concentrations of these three compounds in reaction solution. 91 Overall, no solids or liquids were identified as effective co-oxidants.

Mechanistic Studies Based on Density Functional Theory. DT's involvement in the chemistry is not trivial. DT is primarily known for its ability to perform HAT on alkanes to generate alkyl radicals. In the present case, this could be HAT to convert methane to CH₃●, which has been previously observed.⁶⁸ We initially considered that DT also abstracts H from HTFA to form TFA●. However, HTFA's polarity mismatch with DT⁶¹ and strong O−H BDE (113.7 kcal/

mol) would make HAT of the HTFA O-H bond by DT unlikely. ⁹² If we assume that HCl is generated through HAT from methane by Cl \bullet , it is plausible that DT undergoes a HAT with HCl to regenerate the Cl \bullet . However, the difference in p K_a between H-TFA and H-Cl is >6 units, such that HCl would likely deprotonate to form Cl $^-$. An alternative path for Cl $^-$ would be to undergo electron transfer (ET) with DT $\bullet \bullet$ to again form Cl \bullet and reduce DT $\bullet \bullet$ to DT $\bullet ^-$. ^{85,93} We propose a two-fold involvement of DT in the methane oxidation chemistry. First, active DT $\bullet \bullet$ abstracts hydrogen from CH $_4$ to form CH $_3 \bullet$. Second, DT $\bullet \bullet$ oxidizes Cl $^-$ to Cl \bullet ; Cl \bullet can either directly react with CH $_4$ via HAT or associate with a Cl $^-$ to form a Cl $_2 \bullet ^-$ radical trap. With these considerations in mind, we propose the mechanism depicted in Figure 6.

We probed the mechanism for CH_4 conversion to MeTFA hypothesized in Figure 6 using quantum mechanics (QM) calculations at the DFT level. We begin with the first submechanism, which involves the actual conversion of CH_4 to

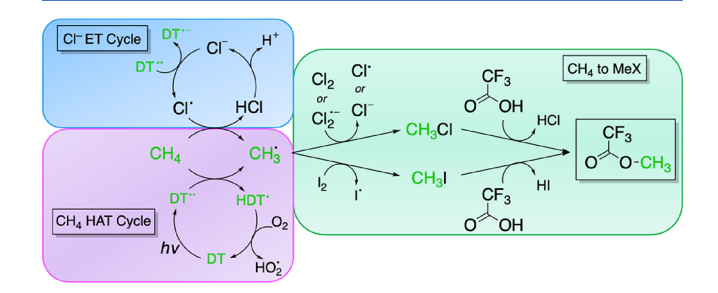


Figure 6. Global mechanism for methane oxidation toward MeX. The mechanism can be partitioned into three sub-mechanisms working synergistically. The first sub-mechanism (green, labeled CH_4 to MeX) is the Cl/I radical-based pathway in which methane (or $CH_3 \bullet$ after HAT) is converted to MeTFA and MeCl (CH_3Cl in figure). The second sub-mechanism (blue, labeled Cl^- ET Cycle) is $DT \bullet \bullet + Cl^-$ ET to generate $Cl \bullet$. The third sub-mechanism (purple, labeled CH_4 HAT Cycle) is the HAT of CH_4 with $DT \bullet \bullet$ or $Cl \bullet$ to generate $CH_3 \bullet$.

MeTFA. With $Cl \bullet$ as the HAT agent and I_2 as the radical trap, the sub-mechanism occurs as:

CH₄ reacts with Cl• to generate CH₃• and HCl CH₃• is then trapped by I₂ to form CH₃I and I• CH₃I reacts with HTFA to form MeTFA and leave HI

The free energy surface for this pathway is detailed in Scheme 3.

Scheme 3. DFT Free Energies at 298 K for the Conversion of Methane to MeTFA within the Cl/I System

Cl-Based Radical Mechanism. The barrier required for HAT between CH₄ and Cl• to produce CH₃• and HCl is calculated to be 1.5 kcal/mol above the methane starting state, while the reaction step is overall downhill by -1.3 kcal/mol. Following formation of CH₃•, molecular I₂ reacts to form CH3I and Io. DFT predicts this step to be barrierless and exergonic by -35.6 kcal/mol, which places CH₃I at -36.9 kcal/mol below the methane starting state. Following the formation of CH3I, MeTFA can now form by a SN2 solvolysis reaction with HTFA. In this reaction step, the protonated O of HTFA acts as a nucleophile to attack the C of CH₃I, forming HTFA⁺-CH₃ and I⁻. The now trivalent O of HTFA⁺-CH₃ gives up H⁺ to I⁻, forming HI and the desired MeTFA product. DFT predicts that this conversion of HTFA and MeI to MeTFA and HI is uphill by 8.9 kcal/mol. The acidity of HI, which should protonate water, would drive the conversion of MeI and HTFA to MeTFA and HI to completion. In this submechanism, the overall conversion of CH_4 to MeTFA is -28.0kcal/mol when Cl \bullet is the HAT agent with I₂ as the radical trap.

We note that although $Cl \bullet$ is recycled in our proposed mechanism, excess KCl optimizes catalyst performance (1.34 mmol of KCl to 0.007 mmol of TBADT at standard aerobic reaction conditions). Likely reasons for this effect are that a higher concentration of Cl^- provides more efficient generation of $Cl \bullet$ via reaction with $DT \bullet \bullet$ and access to other reactive species such as $Cl_2 \bullet^-$ and $Cl_3 - \cdot^{.94}$ In this scenario, excess Cl^- would both increase the production rate of $Cl \bullet$ and increase the pool of these reactive intermediates, which in turn contributes to methane oxidation.

lodine-Free Radical Mechanism. It is important that we also consider the chemistry in the absence of iodine, since this is the condition of some experiments. In the absence of iodine, we observe that oxidation of CH₄ to MeTFA still occurs, however with decreased turnovers. This is likely because without iodine, Cl₂ or Cl₂•⁻ (which forms when Cl• and Cl⁻ associate) serve as the radical trapping agent in which CH₃Cl is formed instead of CH₃I. Because Cl⁻ is a poorer leaving group than I⁻, CH₃Cl + HTFA solvolysis to form HCl and MeTFA is likely retarded. However, HAT between CH₄ and Cl• is not affected by the absence of iodine. The free-energy pathway is depicted in Scheme 4. As noted, HAT between CH₄ and Cl• remains unchanged with a barrier of 1.5 kcal/

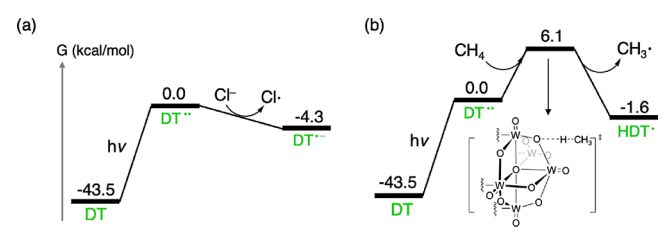
Scheme 4. DFT Free Energies at 298 K for the Conversion of Methane to MeTFA in the Absence of I₂

mol, resulting in the alkyl radical and HCl at -1.3 kcal/mol. Trapping of the alkyl radical with Cl_2 is downhill by -34.0 kcal/mol, resulting in the formation of CH_3Cl at -35.3 kcal/mol. With $\text{Cl}_2\bullet^-$, radical trapping is downhill by -46.3 kcal/mol, resulting in CH_3Cl and Cl^- at -47.6 kcal/mol. Like the case with CH_3I , we propose CH_3Cl follows a S_N2 solvolysis pathway with HTFA to generate MeTFA and HCl. Solvolysis between CH_3Cl and HTFA is uphill 4.7 kcal/mol, resulting in HCl and the desired MeTFA at -30.6 kcal/mol (-42.8 when $\text{Cl}_2\bullet^-$ is the radical trap). While solvolysis with MeCl (4.7 kcal/mol) is thermodynamically more accessible than MeI (8.9 kcal/mol), the actual kinetics for MeCl solvolysis will be slower because the HTFA $^+$ - CH_3 + Cl^- ion pair is less stable than the iodine analogue on account of Cl^- being a worse leaving group than I $^-$.

Decatungstate Integration. Previous reports have shown that ground-state DT, specifically NaDT and TBADT, can be photoexcited by 365-390 nm light to a highly active HAT reagent. 62,73,96,97 The absorption spectrum for DT anion shows a large peak at 324 nm, corresponding to a HOMO-LUMO transition, also marked by ligand-to-metal charge transfer (LMCT). 98,99 This photoexcitation is likely a closed-shell singlet-to-open-shell singlet transition of DT in which the SOMOs reside on the oxygens. The open-shell singlet relaxes from the Franck-Condon point to the open-shell singlet minima in <1 ps. 62 This excited singlet reportedly decays via an intersystem crossing to the active triplet state, which is stabilized by the exchange interaction. This active triplet state is formed with a quantum yield of 0.5–0.6 and exists for 55 \pm 20 ns in acetonitrile. 62,100–105 The triplet state (DT••) has a radical character on the electrophilic oxygens, such that it can readily pull H atoms off neighboring molecules (like CH4 and HCl) to generate radicals when the substrate oxidation potential is above +2.44 V vs saturated calomel electrode (SCE).⁶² When the oxidation potential is below +2.44 V vs SCE, the complex is expected to perform ET; this is the regime in which DT oxidizes Cl⁻ to Cl•. 95 Following ET, protonation of DT• from the medium would result in HDT• with an overall doublet spin. Previously published experimental evidence shows that after reacting, the solution containing DT turns dark blue with strong absorption bands in the 600-800 nm range, which we interpret as the formal reduction of W in DT. 88,93,97,99,106-108 The species responsible for the blue color occurs after relatively long periods of time and is not active in catalysis. For our purposes, we focus on the singlet ground-state DT, the lowest-lying triplet DT., and the reduced HDT.

We calculate that the initial excitation of DT to the lowestlying triplet DT•• requires 43.5 kcal/mol; experimentally, this excitation arises through irradiation by 365–390 nm light. For simplicity, we set DT•• as the reference state of 0.0 kcal/mol in Scheme 5. Spin density analysis reveals significant unpaired spin on the bridging oxygens in DT••. Oddly, the terminal oxo

Scheme 5. DFT Free Energies at 298 K for (a) the Generation of Cl \bullet through ET of Cl $^-$ with DT $\bullet \bullet$ and (b) for the Generation of CH $_3 \bullet$ through HAT of CH $_4$ with DT $\bullet \bullet$



ligands exhibit little spin density, contrary to previous beliefs that the terminal oxos are responsible for HAT.⁶² To confirm this finding, we analyzed the hydrogen binding (HB) energies for the five unique oxygens of DT•• (Figure 7).

DT Site	H-binding Energy (kcal/mol)
1	-29.0
2	-47.3
3	-35.0
4	-47.7
5	-41.4

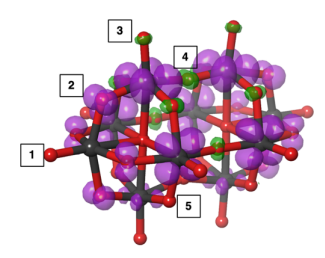


Figure 7. Spin-density diagram for the lowest-lying triplet decatungstate (purple = α , green = β) and hydrogen-binding energies (kcal/mol) for the five unique oxygen sites. The oxygen and tungsten atoms are red and gray, respectively.

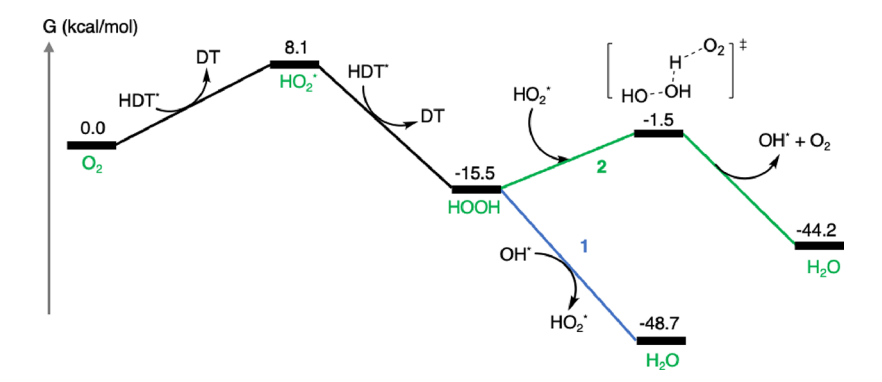
We define the HB energy as the free energy of the reaction $H \bullet + DT \bullet \bullet \to HDT \bullet$. Sites 2, 4, and 5 are bridging oxygens, and sites 1 and 3 are terminal oxo ligands. As the spin density analysis suggests, binding $H \bullet$ to the bridging oxygen sites was most favorable. The HB energy to sites 2, 4, and 5 are -47.3, -47.7, and -41.4 kcal/mol, respectively. In contrast, the HB

energy to sites 1 and 3 are -29.0 and -35.0 kcal/mol, respectively, indicating that binding H to the terminal oxo ligands is significantly less favorable. Overall, site 4 provides the best HB energy, while site 1 is the worst. Thus, site 4 would appear responsible for the HAT since it binds H the strongest, but we note that site 4 is not easily accessible due to the two adjacent oxo groups. For example, CH4 does not readily undergo HAT with site 4 because the adjacent oxo ligands would repel the CH4 due to Pauli repulsion. Instead, we propose that HAT occurs through site 2. Site 2 is easily accessible for HAT and provides the second-best HB energy, only 0.4 kcal/mol less than site 4. Ravelli and coworkers also proposed that site 4 is shielded and therefore not active for HAT.⁶² Site 1 was previously believed to be the active HAT site because it contributes more to the shape of the HOMO-1 orbital compared to site 2 (HOMO-1 is where the unpaired spin resides) and because its geometric parameters match that of HAT with a triplet carbonyl in which the process occurs inplane with the C=O bond. We claim that the difference between sites 1 and 2 for the HOMO-1 contribution is small and that both sites provide geometric parameters suitable for HAT with a carbonyl. This, combined with site 2's more favorable HB energy, leads us to propose that site 2 is responsible for HAT.

Scheme 5 shows ET to DT•• from Cl⁻ to form Cl• and HAT to DT•• from CH₄ to form CH₃•; preceding these steps is the photoexcitation of DT to DT••, which DFT predicts requires 43.5 kcal/mol. For simplicity, we choose DT•• to be the reference state at 0.0 kcal/mol. DFT predicts ET to DT•• from Cl⁻ is downhill by −4.3 kcal/mol. PFT predicts ET, DT•⁻ would protonate to form HDT• (not shown). We find that HAT from CH₄ to DT•• is −1.6 kcal/mol downhill with a transition state barrier of 6.1 kcal/mol above the DT•• reference state. Subsequent regeneration of DT from HDT• is achieved through oxidation by dioxygen.

Decatungstate Regeneration by Dioxygen. HAT leads to the HDT \bullet species, which can undergo further reoxidation to regenerate the DT catalyst and funnel H toward H₂O. Given the presence of dioxygen (O₂) in the reaction vessel, the first step is likely a HAT in which triplet O₂ pulls H off HDT \bullet to generate HO₂ \bullet and a ground-state singlet DT. The HO₂ \bullet can then pull another H off an additional equivalent of HDT \bullet to generate HOOH. We envision that during catalysis, there exists a pool of O–H-containing species such as OH \bullet , HOOH, HO₂ \bullet , etc. These species can react in numerous ways, making it difficult to predict exactly how O₂ and HOOH may funnel toward a thermodynamic sink. However, our previous

Scheme 6. DFT Free Energies at 298 K for the Conversion of Dioxygen to H₂O and Regeneration of the DT Ground State



study on peroxide radical chemistry revealed that in a large ensemble of O–H-containing species, the reactions that occur most are (1) HOOH + OH• \rightarrow HO $_2$ • + H $_2$ O and (2) HOOH + HO $_2$ • \rightarrow OH• + O $_2$ + H $_2$ O. Both reactions consume HOOH and produce H $_2$ O. We hypothesize that upon formation of HOOH from HO $_2$ •, either of these two reactions can consume the HOOH to form H $_2$ O. This H $_2$ O formation mechanism is depicted in Scheme 6.

Starting with triplet O2, HAT to pull H off the doublet HDT• to regenerate ground-state singlet DT while forming HO₂• is uphill by 8.1 kcal/mol. HO₂• can now perform a secondary HAT on an additional HDT• to form HOOH plus another singlet DT; this step is downhill by -15.5 kcal/mol. Formation of HOOH opens numerous avenues for a plethora of possible reaction steps. However, we believe the most likely reactions that can occur are either (1) HOOH + OH \bullet \rightarrow $HO_2 \bullet + H_2O$ or (2) $HOOH + HO_2 \bullet \rightarrow OH \bullet + O_2 + H_2O$. Reaction 1 is barrierless to form HO₂• and H₂O at −48.7 kcal/ mol. Reaction 2 requires a barrier of -1.5 kcal/mol (or 14.0 kcal/mol relative to preceding HOOH intermediate) and is downhill to form OH•, O2, and H2O at -44.2 kcal/mol. Overall, this sub-mechanism converts O2 to H2O and regenerates two ground-state DT from two HDT. We note that this mechanism does not account for DT's reduced -5 or -6 states that are observed in experiment. We believe these states are formed via non-catalytic electron transfer side reactions that do not contribute to the catalytic methane oxidation chemistry. Indeed, previous experimental studies claim that these -5 and -6 states are formed over long time periods and are not catalytic.⁶²

Reaction Tolerance to Water. The DFT-predicted reaction mechanism suggests HO2• formation from the reoxidation of HDT • by O₂, which eventually funnels to the formation of H₂O. Thus, we experimentally probed the reaction tolerance to water. Varying equivalents of water were added at the start of the reaction under our standard aerobic reaction conditions to quantify the effect on the amount of MeX produced. The formation of MeX is plotted against equivalents of added water relative to TBADT in Figure 8. At 1000 equivalents of water relative to TBADT (7.0 mmol of H₂O), there is no effect on MeX production. At 10,000 equivalents of water relative to TBADT (70 mmol of H₂O), MeX production is shut down. At this concentration of water, the impact on reaction rate is likely due to a solvent effect (e.g., reduced acidity) rather than a specific kinetic impact (Figure 8).

SUMMARY AND CONCLUSIONS

We have demonstrated the partial oxidation of methane using a photochemically driven process comprising catalytic TBADT, chloride, and iodine in HTFA. Under aerobic conditions, the MeX yield reached $\sim\!\!9\%$. Our kinetic studies revealed a dependence on dioxygen concentration. Reoxidation experiments with dioxygen led us to achieve methane-to-MeTFA conversion with >350 TOs based on TBADT and $\sim\!\!60\%$ yield based on methane when optimized. MeTFA was shown to be stable under standard reaction conditions, with >94% remaining after 41 h.

Density functional theory calculations were used to determine the reaction mechanism, which validates our proposal that photo and radical chemistry synergistically perform methane functionalization. Based on the DFT calculations and experiments, we propose a radical pathway

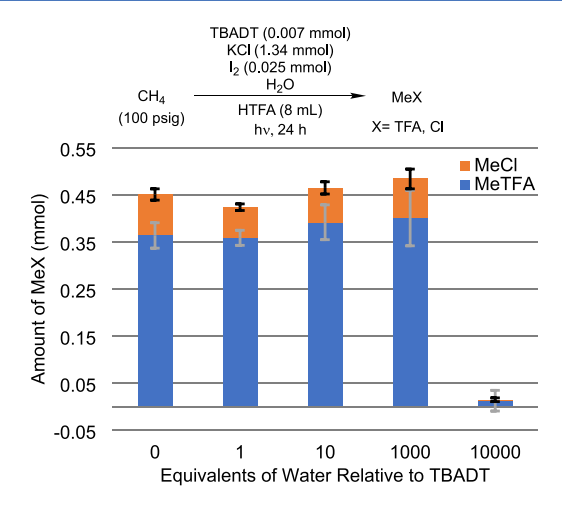


Figure 8. Amount of MeX (X = TFA, Cl) produced under standard aerobic reaction conditions in which varying amounts of water were added to the start of the reaction. Equivalents of water are reported with respect to TBADT. Each bar graph represents the average of at least three independent experiments with error bars depicting the standard deviation of the three experiments.

in which a hydrogen atom is abstracted from methane by a chlorine atom or by triplet DT $\bullet \bullet$ to generate a methyl radical, which is then trapped by some chlorine or iodine species (Cl₂, Cl₂ \bullet^- , and I₂) to generate a methyl halide. From there, HTFA undergoes S_N2 solvolysis with the methyl halide to form the desired ester product, MeTFA. The chlorine radicals in this mechanism are generated through electron transfer from chloride anion to DT $\bullet \bullet$. We propose that after ET by DT $\bullet \bullet$ and subsequent protonation, dioxygen reoxidizes HDT \bullet and subsequently forms water.

The addition of DT to the chloride—iodine system presents a novel strategy for the photodriven partial oxidation of methane toward MeTFA. DT's remarkable quantum efficiency and HAT reactivity provides synergy with the free radical chemistry of chloride and iodine, affording the desired MeTFA product which maintains excellent stability.

EXPERIMENTAL SECTION

Caution. Many of the reagents and conditions described herein are particularly hazardous. Appropriate safety measures should be taken and appropriate personal protective equipment should be worn when handling strong acids, especially in large volumes. Broadband mercury arc lamps are dangerous to the skin and eyes, and even a brief exposure can result in permanent damage. The lamps must only be turned on while encased in an enclosure that precludes exposure to the naked eye. Cool to room-temperature water must always be recirculated around the lamp to prevent uncontrolled overheating; this is especially important when conducting reactions containing mixtures of methane and air or dioxygen. NOTE: Mixtures of methane and dioxygen are potentially explosive. 111

General Comments and Materials. All reactions were carried out under an ambient atmosphere unless indicated otherwise. Methane, oxygen, nitrogen, and argon were purchased from GTS-Welco and used as received. Potassium chloride, potassium bromide, iodine, trifluoroacetic acid (>99.9%), glacial acetic acid, nitromethane, copper(II) acetate hydrate, copper(II) chloride hydrate, copper(II) trifluoroacetate hydrate, potassium persulfate, di-tert-butyl peroxide, tert-butyl hydroperoxide, hydrogen peroxide, and trifluoroacetic

anhydride were purchased commercially and used as received. Tetrabutylammonium decatungstate (TBADT) was synthesized and characterized according to a literature procedure, for which the reagents were purchased commercially and used as received. High-pressure reaction vessels were constructed from Fisher-Porter tubes purchased from Andrews Glass, and custom-built reactor tops were constructed from Swagelok stainless steel fittings (see Figure S2). These reaction vessels can be safely pressurized to 250 psig at room temperature. The photolysis enclosure was constructed with a power supply feeding a broadband mercury arc lamp. The mercury arc lamp was nested in a quartz immersion well in which cool to roomtemperature DI water (15-40 °C) was recirculated through at all times the lamp was powered on. The power supply (450 watts, product #7830-60), Hanovia mercury arc lamp (medium pressure, 450 watt, 121.92 mm arc length, 244.35 mm overall length, product #7825-34), and quartz immersion well (product #7854-27) were purchased from Ace Glass. The mercury arc lamp is quoted to irradiate ~40-48% in the ultraviolet spectral range, ~40-43% in the visible spectral range, and the remainder in the infrared spectral range. Mercury arc lamps were replaced every 1000 h. NMR analysis was performed using a Varian Inova 500 or 600 MHz spectrometer. ¹H NMR data of reaction mixtures were obtained with a capillary of C₆D₆ as the internal lock reference. Chemical shifts are reported relative to the internal standards of either CH₃NO₂ (δ 4.18) or HOAc (δ 2.04). UV-vis spectral measurements of TBADT were collected on a Cary 60 UV-vis spectrometer. Samples were prepared in 1 cm square quartz cuvettes.

General Procedure for Photochemical Methane Functionalization. Reactions were performed in triplicate and at room temperature. Each Fisher-Porter reactor was charged with a stir bar and solid reagents (TBADT, KCl, and I₂) followed by 8 mL of HTFA. Unless specified otherwise, TBADT was ground with a mortar and pestle prior to addition to the reactor. The reactors were sealed under air and weighed. The reactors were then pressurized with methane and weighed again. The amount of methane added was quantified by the difference in mass before and after methane addition. The reactors were then added to a photolysis enclosure, each positioned 16 cm from the mercury arc lamp with uniform stirring. Reaction time was started 15 min following lamp turnon to account for lamp warm-up time to reach full intensity. After the reaction, the lamp was turned off and the photolysis chamber was kept closed for at least 1 min to ensure that the lamp was safely powered off. The reactors were removed, weighed to probe for leaks, and cooled in front of a fan for at least 15 min. The reactors were then vented in a fume hood, 20 μ L of internal standard (either CH₃NO₂ or HOAc) was added to each reaction, and the reaction mixtures were thoroughly stirred. An aliquot from each reaction mixture was removed and centrifuged, from which the supernatant of each was added to an NMR tube containing a sealed capillary containing C₆D₆. The products were analyzed by ¹H NMR spectroscopy. See Figure S1 for a sample ¹H NMR spectrum.

MeTFA Stability under Photochemical Conditions. Reactions were performed in triplicate and at room temperature. Each Fisher–Porter reactor was charged with 0.007 mmol of TBADT, 1.34 mmol of KCl, 0.025 mmol of I₂, and a stir bar followed by 8 mL of HTFA and 0.35 mmol of MeTFA. The reactors were sealed under air, pressurized with 100 psig of Ar, and weighed. The reactors were then added to a

photolysis enclosure, each positioned 16 cm from the mercury arc lamp, with uniform stirring. Reaction time was started 15 min following lamp turn-on to account for lamp warm-up time to reach full intensity. After the reaction, the lamp was turned off and the photolysis chamber was kept closed for at least 1 min to ensure that the lamp was safely powered off. The reactors were removed, weighed to probe for leaks, and cooled in front of a fan for at least 15 min. The reactors were then vented in a fume hood, 20 μ L of internal standard (either CH₃NO₂ or HOAc) was added to each reaction, and the reaction mixtures were thoroughly stirred. An aliquot from each reaction mixture was removed and centrifuged, from which the supernatant of each was added to an NMR tube containing a sealed capillary containing C₆D₆. The products were analyzed by ¹H NMR spectroscopy.

Experiments Involving Dinitrogen/Dioxygen Purges. Reactions were performed in triplicate and at room temperature. Each Fisher-Porter reactor was charged with 0.007 mmol of TBADT, 1.34 mmol of KCl, 0.025 mmol of I₂, and a stir bar followed by 8 mL of HTFA. The reactor tops were fitted to the reactors but not sealed. Using a long needle, the respective gas was bubbled through each reaction solution one at a time. Following 1 min of bubbling, the needle was removed and the reactor valve was quickly sealed. The reactors were weighed, pressurized with 100 psig of methane, and weighed again. The amount of methane added was quantified by the difference in mass before and after methane addition. The reactors were then added to a photolysis enclosure, each positioned 16 cm from the mercury arc lamp, with uniform stirring. Reaction time was started 15 min following lamp turnon to account for lamp warm-up time to reach full intensity. After 24 h of reaction, the lamp was turned off and the photolysis chamber was kept closed for at least 1 min to ensure that the lamp was safely powered off. The reactors were removed, weighed to probe for leaks, and cooled in front of a fan for at least 15 min. The reactors were then vented in a fume hood, 20 µL of internal standard (either CH₃NO₂ or HOAc) was added to each reaction, and the reaction mixtures were thoroughly stirred. An aliquot from each reaction mixture was removed and centrifuged, from which the supernatant of each was added to an NMR tube containing a sealed capillary containing C₆D₆. The products were analyzed by ¹H NMR

Reoxidation Experiments with Dioxygen. Reactions were performed in triplicate and at room temperature. Each Fisher-Porter reactor was charged with 0.007 mmol of TBADT, 1.34 mmol of KCl, 0.025 mmol of I2, and a stir bar followed by 8 mL of HTFA. Reactors were either sealed under air or purged with dioxygen. The reactors were weighed, pressurized with methane, and weighed again. The amount of methane added was quantified by the difference in mass before and after methane addition. The reactors were then added to a photolysis enclosure, each positioned 16 cm from the mercury arc lamp, with uniform stirring. Reaction time was started 15 min following lamp turn-on to account for lamp warm-up time to reach full intensity. After the reaction, the lamp was turned off and the photolysis chamber was kept closed for at least 1 min to ensure that the lamp was safely powered off. The reactors were removed, weighed to probe for leaks, and cooled in front of a fan for at least 15 min. The reactors were then pressurized with dioxygen top pressure and weighed again. The amount of dioxygen added was quantified by the difference in mass before and after dioxygen addition. The reactors were

ACS Catalysis pubs.acs.org/acscatalysis Research Article

then subjected again to the mercury arc lamp. This process of adding additional dioxygen top pressure and re-subjecting to the mercury arc lamp was repeated as detailed in each set of reaction conditions. Following the last dioxygen addition and irradiation, the reactors were removed, weighed to probe for leaks, and cooled in front of a fan for at least 15 min. The reactors were then vented in a fume hood, 20 μL of internal standard (either CH_3NO_2 or HOAc) was added to each reaction, and the reaction mixtures were thoroughly stirred. An aliquot from each reaction mixture was removed and centrifuged, from which the supernatant of each was added to an NMR tube containing a sealed capillary containing C_6D_6 . The products were analyzed by 1H NMR spectroscopy.

Computational Details. All density functional theory calculations were performed within the Jaguar software package version 10.9 from Schrodinger Inc. Structures were first optimized using the PBE flavor of DFT including the Grimme-Becke-Johnson (GBJ) D3 correction for London dispersion. W and I atoms were treated with the Los Alamos large-core triple-zeta pseudopotential augmented with polarization and diffuse functions (LAV3P* + in Jaguar). All other atoms were treated with the 6-31 + G(d) basis set. PBE-D3 geometry optimizations were followed by additional singlepoint energy (SPE) calculations with implicit solvent. SPEs were calculated with the M06-2X functional using GBJ D3 dispersion correction. For the SPE, W and I were described with the Los Alamos small-core triple-zeta potential augmented with polarization and diffuse functions (LACV3P**++ in Jaguar); all other atoms were described with the 6-311+ +G(d,p) basis set. Solvent effects were included through the PBF Poisson Boltzmann continuum model with parameters matching trifluoroacetic acid. Frequency calculations were performed at the M06-2X-D3/LACV3P**++ level to predict thermochemical properties (zero-point energy, entropy, and temperature correction to enthalpy). Frequency calculations also served to confirm intermediates (0 imaginary frequencies) and transition states (single imaginary frequency).

ASSOCIATED CONTENT

Supporting Information

The Supporting Information is available free of charge at https://pubs.acs.org/doi/10.1021/acscatal.3c00750.

Supplementary catalytic and stability assessments, NMR spectra, additional DFT calculations, and DFT free energies (PDF)

DT structures (XYZ)

AUTHOR INFORMATION

Corresponding Authors

John T. Groves — Department of Chemistry, Princeton University, Princeton, New Jersey 08544, United States; orcid.org/0000-0002-9944-5899; Email: jtgroves@princeton.edu

William A. Goddard III — Materials and Process Simulation Center, California Institute of Technology, Pasadena, California 91125, United States; ⊚ orcid.org/0000-0003-0097-5716; Email: wag@caltech.edu

T. Brent Gunnoe — Department of Chemistry, University of Virginia, Charlottesville, Virginia 22904, United States;
o orcid.org/0000-0001-5714-3887; Email: tbg7h@virginia.edu

Authors

Charles B. Musgrave III — Materials and Process Simulation Center, California Institute of Technology, Pasadena, California 91125, United States; orcid.org/0000-0002-3432-0817

Kaeleigh Olsen — Department of Chemistry, University of Virginia, Charlottesville, Virginia 22904, United States Nichole S. Liebov — Department of Chemistry, University of Virginia, Charlottesville, Virginia 22904, United States

Complete contact information is available at: https://pubs.acs.org/10.1021/acscatal.3c00750

Author Contributions

[#]C.B.M. and K.O. contributed equally to this work.

Notes

The authors declare no competing financial interest.

ACKNOWLEDGMENTS

This research was sponsored by the U.S. Department of Energy, Office of Energy Efficiency and Renewable Energy, Advanced Manufacturing Office, under contract DE-AC05-00OR22725 with UT-Battelle, LLC. W.A.G. acknowledges support by the Liquid Sunlight Alliance, which is supported by the U.S. Department of Energy, Office of Science, Office of Basic Energy Sciences, Fuels from Sunlight Hub under Award Number DE-SC0021266. Partial support of this research during the writing by the National Science Foundation (CHE-1464578 to J.T.G.) is gratefully acknowledged.

REFERENCES

- (1) Olah, G. A.; Goeppert, A.; Prakash, G. K. S. Beyond Oil and Gas: The Methanol Economy; Wiley-VCH: Weinheim, Germany, 2009.
- (2) Gunsalus, N. J.; Koppaka, A.; Park, S. H.; Bischof, S. M.; Hashiguchi, B. G.; Periana, R. A. Homogeneous Functionalization of Methane. *Chem. Rev.* **2017**, *117*, 8521–8573.
- (3) Dummer, N. F.; Willock, D. J.; He, Q.; Howard, M. J.; Lewis, R. J.; Qi, G.; Taylor, S. H.; Xu, J.; Bethell, D.; Kiely, C. J.; Hutchings, G. J. Methane Oxidation to Methanol. *Chem. Rev.* **2022**, DOI: 10.1021/acs.chemrev.2c00439.
- (4) BP Statistical Review of World Energy 2022; 71st ed.; BP: London, 2022.
- (5) Zakaria, Z.; Kamarudin, S. K. Direct conversion technologies of methane to methanol: An overview. *Renewable Sustainable Energy Rev.* **2016**, *65*, 250–261.
- (6) Schwach, P.; Pan, X.; Bao, X. Direct Conversion of Methane to Value-Added Chemicals over Heterogeneous Catalysts: Challenges and Prospects. *Chem. Rev.* **2017**, *117*, 8497–8520.
- (7) Tang, P.; Zhu, Q.; Wu, Z.; Ma, D. Methane activation: the past and future. *Energy Environ. Sci.* **2014**, *7*, 2580–2591.
- (8) Ravi, M.; Ranocchiari, M.; van Bokhoven, J. A. The Direct Catalytic Oxidation of Methane to Methanol—A Critical Assessment. *Angew. Chem., Int. Ed.* **2017**, *56*, 16464–16483.
- (9) Lin, R.; Amrute, A. P.; Pérez-Ramírez, J. Halogen-Mediated Conversion of Hydrocarbons to Commodities. *Chem. Rev.* **2017**, *117*, 4182–4247.
- (10) Zichittella, G.; Paunović, V.; Amrute, A. P.; Pérez-Ramírez, J. Catalytic Oxychlorination versus Oxybromination for Methane Functionalization. *ACS Catal.* **2017**, *7*, 1805–1817.
- (11) Podkolzin, S. G.; Stangland, E. E.; Jones, M. E.; Peringer, E.; Lercher, J. A. Methyl Chloride Production from Methane over Lanthanum-Based Catalysts. *J. Am. Chem. Soc.* **2007**, *129*, 2569–2576. (12) Wang, K. X.; Xu, H. F.; Li, W. S.; Zhou, X. P. Acetic acid synthesis from methane by non-synthesis gas process. *J. Mol. Catal. A: Chem.* **2005**, 225, 65–69.

- (13) Paunović, V.; Zichittella, G.; Moser, M.; Amrute, A. P.; Pérez-Ramírez, J. Catalyst design for natural-gas upgrading through oxybromination chemistry. *Nat. Chem.* **2016**, *8*, 803–809.
- (14) Tschuikow-Roux, E.; Paddison, S. Bond dissociation energies and radical heats of formation in CH₃Cl, CH₂Cl₂, CH₃Br, CH₂Br₂, CH₃FCl, and CHFCl₂. *Int. J. Chem. Kinet.* **1987**, *19*, 15–24.
- (15) McGivern, W. S.; Derecskei-Kovacs, A.; North, S. W.; Francisco, J. S. Computationally Efficient Methodology To Calculate C–H and C–X (X = F, Cl, and Br) Bond Dissociation Energies in Haloalkanes. *J. Phys. Chem. A* **2000**, *104*, 7916–7916.
- (16) Breed, A.; Doherty, M. F.; Gadewar, S.; Grosso, P.; Lorkovic, I. M.; McFarland, E. W.; Weiss, M. J. Natural gas conversion to liquid fuels in a zone reactor. *Catal. Today* **2005**, *106*, 301–304.
- (17) Shilov, A. E.; Shul'pin, G. B. Activation of C-H Bonds by Metal Complexes. *Chem. Rev.* 1997, 97, 2879–2932.
- (18) Periana, R. A.; Taube, D. J.; Gamble, S.; Taube, H.; Satoh, T.; Fujii, H. Platinum Catalysts for the High-Yield Oxidation of Methane to a Methanol Derivative. *Science* **1998**, *280*, 560–564.
- (19) Chen, S.-S.; Koppaka, A.; Periana, R. A.; Ess, D. H. Theory and Experiment Demonstrate that Sb(V)-Promoted Methane C–H Activation and Functionalization Outcompete Superacid Protonolysis in Sulfuric Acid. *J. Am. Chem. Soc.* **2021**, *143*, 18242–18250.
- (20) Periana, R. A.; Mirinov, O.; Taube, D. J.; Gamble, S. High yield conversion of methane to methyl bisulfate catalyzed by iodine cations. *Chem. Commun.* **2002**, 2376–2377.
- (21) Gang, X.; Zhu, Y.; Birch, H.; Hjuler, H. A.; Bjerrum, N. J. Iodine as catalyst for the direct oxidation of methane to methyl sulfates in oleum. *Appl. Catal. A* **2004**, *261*, 91–98.
- (22) Hashiguchi, B. G.; Konnick, M. M.; Bischof, S. M.; Gustafson, S. J.; Devarajan, D.; Gunsalus, N.; Ess, D. H.; Periana, R. A. Main-Group Compounds Selectively Oxidize Mixtures of Methane Ethane, and Propane to Alcohol Esters. *Science* **2014**, *343*, 1232–1237.
- (23) Groothaert, M. H.; Smeets, P. J.; Sels, B. F.; Jacobs, P. A.; Schoonheydt, R. A. Selective Oxidation of Methane by the Bis(μ -oxo)dicopper Core Stabilized on ZSM-5 and Mordenite Zeolites. *J. Am. Chem. Soc.* **2005**, *127*, 1394–1395.
- (24) Woertink, J. S.; Smeets, P. J.; Groothaert, M. H.; Vance, M. A.; Sels, B. F.; Schoonheydt, R. A.; Solomon, E. I. A [Cu₂O]²⁺ core in Cu-ZSM-5, the active site in the oxidation of methane to methanol. *Proc. Natl. Acad. Scic. USA* **2009**, *106*, 18908–18913.
- (25) Alayon, E. M.; Nachtegaal, M.; Ranocchiari, M.; van Bokhoven, J. A. Catalytic conversion of methane to methanol over Cumordenite. *Chem. Commun.* **2012**, *48*, 404–406.
- (26) Vanelderen, P.; Snyder, B. E.; Tsai, M. L.; Hadt, R. G.; Vancauwenbergh, J.; Coussens, O.; Schoonheydt, R. A.; Sels, B. F.; Solomon, E. I. Spectroscopic definition of the copper active sites in mordenite: selective methane oxidation. *J. Am. Chem. Soc.* **2015**, *137*, 6383–6392.
- (27) Grundner, S.; Markovits, M. A. C.; Li, G.; Tromp, M.; Pidko, E. A.; Hensen, E. J.; Jentys, A.; Sanchez-Sanchez, M.; Lercher, J. A. Single-site trinuclear copper oxygen clusters in mordenite for selective conversion of methane to methanol. *Nat. Commun.* **2015**, *6*, 7546.
- (28) Ipek, B.; Lobo, R. F. Catalytic conversion of methane to methanol on Cu-SSZ-13 using N_2O as oxidant. *Chem. Commun.* **2016**, 52, 13401–13404.
- (29) Pappas, D. K.; Martini, A.; Dyballa, M.; Kvande, K.; Teketel, S.; Lomachenko, K. A.; Baran, R.; Glatzel, P.; Arstad, B.; Berlier, G.; Lamberti, C.; Bordiga, S.; Olsbye, U.; Svelle, S.; Beato, P.; Borfecchia, E. The Nuclearity of the Active Site for Methane to Methanol Conversion in Cu-Mordenite: A Quantitative Assessment. *J. Am. Chem. Soc.* **2018**, *140*, 15270–15278.
- (30) Brezicki, G.; Kammert, J. D.; Gunnoe, T. B.; Paolucci, C.; Davis, R. J. Insights into the Speciation of Cu in the Cu-H-Mordenite Catalyst for the Oxidation of Methane to Methanol. *ACS Catal.* **2019**, 9, 5308–5319.
- (31) Kulkarni, A. R.; Zhao, Z.-J.; Siahrostami, S.; Nørskov, J. K.; Studt, F. Cation-exchanged zeolites for the selective oxidation of methane to methanol. *Catal. Sci. Technol.* **2018**, *8*, 114–123.

- (32) Walling, C.; Mayahi, M. F. Some Solvent and Structural Effects in Free Radical Chlorination. *J. Am. Chem. Soc.* **1959**, *81*, 1485–1489.
- (33) Tedder, J. M. Which Factors Determine the Reactivity and Regioselectivity of Free Radical Substitution and Addition Reactions? *Angew. Chem., Int. Ed.* **1982**, 21, 401–410.
- (34) Fortman, G. C.; Boaz, N. C.; Munz, D.; Konnick, M. M.; Periana, R. A.; Groves, J. T.; Gunnoe, T. B. Selective monooxidation of light alkanes using chloride and iodate. *J. Am. Chem. Soc.* **2014**, *136*, 8393–8401.
- (35) Kalman, S. E.; Munz, D.; Fortman, G. C.; Boaz, N. C.; Groves, J. T.; Gunnoe, T. B. Partial oxidation of light alkanes by periodate and chloride salts. *Dalton Trans.* **2015**, *44*, 5294–5298.
- (36) Schwartz, N. A.; Boaz, N. C.; Kalman, S. E.; Zhuang, T.; Goldberg, J. M.; Fu, R.; Nielsen, R. J.; Goddard, W. A.; Groves, J. T.; Gunnoe, T. B. Mechanism of Hydrocarbon Functionalization by an Iodate/Chloride System: The Role of Ester Protection. *ACS Catal.* **2018**, *8*, 3138–3149.
- (37) Fu, R.; Nielsen, R. J.; Liebov, N. S.; Goddard, W. A.; Gunnoe, T. B.; Groves, J. T. DFT Mechanistic Study of Methane Mono-Esterification by Hypervalent Iodine Alkane Oxidation Process. *J. Phys. Chem. C* **2019**, *123*, 15674–15684.
- (38) Vargaftik, M. N.; Stolarov, I. P.; Moiseev, I. I. Highly selective partial oxidation of methane to methyl trifluoroacetate. *J. Chem. Soc., Chem. Commun.* **1990**, 1049–1050.
- (39) Chen, W.; Kocal, J. A.; Brandvold, T. A.; Bricker, M. L.; Bare, S. R.; Broach, R. W.; Greenlay, N.; Popp, K.; Walenga, J. T.; Yang, S. S.; Low, J. J. Manganese oxide catalyzed methane partial oxidation in trifluoroacetic acid: Catalysis and kinetic analysis. *Catal. Today* **2009**, 140, 157–161.
- (40) Tang, R.; Kochi, J. K. Cobalt(III) trifluoroacetate: An electron transfer oxidant. *J. Inorg. Nucl. Chem.* **1973**, *35*, 3845–3856.
- (41) Coutard, N.; Musgrave, C. B., III; Moon, J.; Liebov, N. S.; Nielsen, R. M.; Goldberg, J. M.; Li, M.; Jia, X.; Lee, S.; Dickie, D. A.; Schinski, W. L.; Wu, Z.; Groves, J. T.; Goddard, W. A., III; Gunnoe, T. B. Manganese Catalyzed Partial Oxidation of Light Alkanes. *ACS Catal.* 2022, *12*, 5356–5370.
- (42) Deng, H. P.; Zhou, Q.; Wu, J. Microtubing-Reactor-Assisted Aliphatic C-H Functionalization with HCl as a Hydrogen-Atom-Transfer Catalyst Precursor in Conjunction with an Organic Photoredox Catalyst. *Angew. Chem., Int. Ed.* **2018**, *57*, 12661–12665.
- (43) Gonzalez, M. I.; Gygi, D.; Qin, Y.; Zhu, Q.; Johnson, E. J.; Chen, Y.-S.; Nocera, D. G. Taming the Chlorine Radical: Enforcing Steric Control over Chlorine-Radical-Mediated C–H Activation. J. Am. Chem. Soc. 2022, 144, 1464–1472.
- (44) Yang, Q. M.; Wang, Y.-H.; Qiao, Y.; Gau, M.; Carroll, P. J.; Walsh, P. J.; Schelter, E. J. Photocatalytic C–H activation and the subtle role of chlorine radical complexation in reactivity. *Science* **2021**, 372, 847.
- (45) Li, Z.; Luo, L.; Li, M.; Chen, W.; Liu, Y.; Yang, J.; Xu, S.-M.; Zhou, H.; Ma, L.; Xu, M.; Kong, X.; Duan, H. Photoelectrocatalytic C–H halogenation over an oxygen vacancy-rich TiO₂ photoanode. *Nat. Commun.* **2021**, *12*, 6698.
- (46) Panetti, G. B.; Yang, Q.; Gau, M. R.; Carroll, P. J.; Walsh, P. J.; Schelter, E. J. Discovery and mechanistic investigation of photo-induced sp³ C–H activation of hydrocarbons by the simple anion hexachlorotitanate. *Chem. Catal.* **2022**, *2*, 853–866.
- (47) Coutard, N.; Goldberg, J. M.; Valle, H. U.; Cao, Y.; Jia, X.; Jeffrey, P. D.; Gunnoe, T. B.; Groves, J. T. Aerobic Partial Oxidation of Alkanes Using Photodriven Iron Catalysis. *Inorg. Chem.* **2022**, *61*, 759–766.
- (48) Liebov, N. S.; Goldberg, J. M.; Boaz, N. C.; Coutard, N.; Kalman, S. E.; Zhuang, T.; Groves, J. T.; Gunnoe, T. B. Selective Photo-Oxygenation of Light Alkanes Using Iodine Oxides and Chloride. *ChemCatChem* **2019**, *11*, 5045–5054.
- (49) Zhang, Q.; Liu, S.; Lei, J.; Zhang, Y.; Meng, C.; Duan, C.; Jin, Y. Iron-Catalyzed Photoredox Functionalization of Methane and Heavier Gaseous Alkanes: Scope, Kinetics, and Computational Studies. Org. Lett. 2022, 24, 1901–1906.

- (50) Hirscher, N. A.; Ohri, N.; Yang, Q.; Zhou, J.; Anna, J. M.; Schelter, E. J.; Goldberg, K. I. A Metal-Free, Photocatalytic Method for Aerobic Alkane Iodination. *J. Am. Chem. Soc.* **2021**, *143*, 19262–19267.
- (51) Gumerova, N. I.; Rompel, A. Synthesis, structures and applications of electron-rich polyoxometalates. *Nat. Rev. Chem.* 2018. 2.
- (52) Pope, M. T.; Müller, A. Polyoxometalate Chemistry: An Old Field with New Dimensions in Several Disciplines. *Angew. Chem., Int. Ed.* **1991**, *30*, 34–48.
- (53) Long, D.-L.; Burkholder, E.; Cronin, L. Polyoxometalate clusters, nanostructures and materials: From self assembly to designer materials and devices. *Chem. Soc. Rev.* **2007**, *36*, 105–121.
- (54) Dupré, N.; Rémy, P.; Micoine, K.; Boglio, C.; Thorimbert, S.; Lacôte, E.; Hasenknopf, B.; Malacria, M. Chemoselective Catalysis with Organosoluble Lewis Acidic Polyoxotungstates. *Chem. Eur. J.* **2010**, *16*, 7256–7264.
- (55) Bar-Nahum, I.; Khenkin, A. M.; Neumann, R. Mild, Aqueous, Aerobic, Catalytic Oxidation of Methane to Methanol and Acetaldehyde Catalyzed by a Supported Bipyrimidinylplatinum—Polyoxometalate Hybrid Compound. *J. Am. Chem. Soc.* **2004**, *126*, 10236–10237.
- (56) Skjelstad, B. B.; Helgaker, T.; Maeda, S.; Balcells, D. Oxyl Character and Methane Hydroxylation Mechanism in Heterometallic $M(O)Co_3O_4$ Cubanes (M = Cr, Mn, Fe, Mo, Tc, Ru, and Rh). ACS Catal. 2022, 12, 12326–12335.
- (57) Wang, S.-S.; Yang, G.-Y. Recent Advances in Polyoxometalate-Catalyzed Reactions. Chem. Rev. 2015, 115, 4893-4962.
- (58) Hill, C. L. Progress and challenges in polyoxometalate-based catalysis and catalytic materials chemistry. *J. Mol. Catal. A: Chem.* **2007**, 262, 2–6.
- (59) Tzirakis, M. D.; Lykakis, I. N.; Orfanopoulos, M. Decatungstate as an efficient photocatalyst in organic chemistry. *Chem. Soc. Rev.* **2009**, *38*, 2609–2621.
- (60) Ravelli, D.; Protti, S.; Fagnoni, M. Decatungstate Anion for Photocatalyzed "Window Ledge" Reactions. *Acc. Chem. Res.* **2016**, *49*, 2232–2242.
- (61) Ravelli, D.; Fagnoni, M.; Fukuyama, T.; Nishikawa, T.; Ryu, I. Site-Selective C–H Functionalization by Decatungstate Anion Photocatalysis: Synergistic Control by Polar and Steric Effects Expands the Reaction Scope. *ACS Catal.* **2018**, *8*, 701–713.
- (62) De Waele, V.; Poizat, O.; Fagnoni, M.; Bagno, A.; Ravelli, D. Unraveling the Key Features of the Reactive State of Decatungstate Anion in Hydrogen Atom Transfer (HAT) Photocatalysis. *ACS Catal.* **2016**, *6*, 7174–7182.
- (63) Cheung, K. P. S.; Sarkar, S.; Gevorgyan, V. Visible Light-Induced Transition Metal Catalysis. *Chem. Rev.* **2022**, *122*, 1543–1625.
- (64) Holmberg-Douglas, N.; Nicewicz, D. A. Photoredox-Catalyzed C-H Functionalization Reactions. *Chem. Rev.* **2022**, *122*, 1925–2016.
- (65) Sarver, P. J.; Bacauanu, V.; Schultz, D. M.; DiRocco, D. A.; Lam, Y. H.; Sherer, E. C.; MacMillan, D. W. C. The merger of decatungstate and copper catalysis to enable aliphatic C(sp³)-H trifluoromethylation. *Nat. Chem.* **2020**, *12*, 459–467.
- (66) Schultz, D. M.; Lévesque, F.; DiRocco, D. A.; Reibarkh, M.; Ji, Y.; Joyce, L. A.; Dropinski, J. F.; Sheng, H.; Sherry, B. D.; Davies, I. W. Oxyfunctionalization of the Remote C–H Bonds of Aliphatic Amines by Decatungstate Photocatalysis. *Angew. Chem., Int. Ed.* **2017**, 56, 15274–15278.
- (67) Wu, W.; Fu, Z.; Tang, S.; Zou, S.; Wen, X.; Meng, Y.; Sun, S.; Deng, J.; Liu, Y.; Yin, D. $(nBu_4N)_4W_{10}O_{32}$ -catalyzed selective oxygenation of cyclohexane by molecular oxygen under visible light irradiation. *Appl. Catal. B* **2015**, *164*, 113–119.
- (68) Laudadio, G.; Deng, Y.; van der Wal, K.; Ravelli, D.; Nuño, M.; Fagnoni, M.; Guthrie, D.; Sun, Y.; Noël, T. $C(sp^3)$ –H functionalizations of light hydrocarbons using decatungstate photocatalysis in flow. *Science* **2020**, *369*, 92–96.
- (69) Laudadio, G.; Govaerts, S.; Wang, Y.; Ravelli, D.; Koolman, H. F.; Fagnoni, M.; Djuric, S. W.; Noël, T. Selective $C(sp^3)$ —H Aerobic

- Oxidation Enabled by Decatungstate Photocatalysis in Flow. *Angew. Chem., Int. Ed.* **2018**, *57*, 4078–4082.
- (70) Halperin, S. D.; Fan, H.; Chang, S.; Martin, R. E.; Britton, R. A Convenient Photocatalytic Fluorination of Unactivated C–H Bonds. *Angew. Chem., Int. Ed.* **2014**, *53*, 4690–4693.
- (71) Perry, I. B.; Brewer, T. F.; Sarver, P. J.; Schultz, D. M.; DiRocco, D. A.; MacMillan, D. W. C. Direct arylation of strong aliphatic C–H bonds. *Nature* **2018**, *560*, 70–75.
- (72) Murphy, J. J.; Bastida, D.; Paria, S.; Fagnoni, M.; Melchiorre, P. Asymmetric catalytic formation of quaternary carbons by iminium ion trapping of radicals. *Nature* **2016**, *532*, 218–222.
- (73) Zeng, J.; Torigoe, T.; Kuninobu, Y. Control of Site-Selectivity in Hydrogen Atom Transfer by Electrostatic Interaction: Proximal-Selective C(sp³)–H Alkylation of 2-Methylanilinium Salts Using a Decatungstate Photocatalyst. *ACS Catal.* **2022**, *12*, 3058–3062.
- (74) Capaldo, L.; Bonciolini, S.; Pulcinella, A.; Nuño, M.; Noël, T. Modular allylation of C(sp³)—H bonds by combining decatungstate photocatalysis and HWE olefination in flow. *Chem. Sci.* **2022**, *13*, 7325–7331.
- (75) Wang, Y.-T.; Shih, Y.-L.; Wu, Y.-K.; Ryu, I. Site-Selective C(sp³)—H Alkenylation Using Decatungstate Anion as Photocatalyst. *Adv. Syn. Catal.* **2022**, *364*, 1039—1043.
- (76) Capaldo, L.; Ravelli, D.; Fagnoni, M. Direct Photocatalyzed Hydrogen Atom Transfer (HAT) for Aliphatic C-H Bonds Elaboration. *Chem. Rev.* **2022**, 122, 1875–1924.
- (77) Golden, D. L.; Suh, S. E.; Stahl, S. S. Radical C(sp³)–H functionalization and cross-coupling reactions. *Nat. Rev. Chem.* **2022**, *6*, 405–427.
- (78) Pulcinella, A.; Mazzarella, D.; Noël, T. Homogeneous catalytic $C(sp^3)$ –H functionalization of gaseous alkanes. *Chem. Commun.* **2021**, *57*, 9956–9967.
- (79) Ye, Z.; Lin, Y.-M.; Gong, L. The Merger of Photocatalyzed Hydrogen Atom Transfer with Transition Metal Catalysis for C-H Functionalization of Alkanes and Cycloalkanes. *Eur. J. Org. Chem.* **2021**, 2021, 5545–5556.
- (80) Wang, Y.-H.; Yang, Q.; Walsh, P. J.; Schelter, E. J. Light-mediated aerobic oxidation of C(sp³)-H bonds by a Ce(IV) hexachloride complex. *Org. Chem. Front.* **2022**, *9*, 2612–2620.
- (81) Gygi, D.; Gonzalez, M. I.; Hwang, S. J.; Xia, K. T.; Qin, Y. Z.; Johnson, E. J.; Gygi, F.; Chen, Y. S.; Nocera, D. G. Capturing the Complete Reaction Profile of a C–H Bond Activation. *J. Am. Chem. Soc.* 2021, 143, 6060–6064.
- (82) Troian-Gautier, L.; Turlington, M. D.; Wehlin, S. A. M.; Maurer, A. B.; Brady, M. D.; Swords, W. B.; Meyer, G. J. Halide Photoredox Chemistry. *Chem. Rev.* **2019**, *119*, 4628–4683.
- (83) Shields, B. J.; Doyle, A. G. Direct C(sp³)—H Cross Coupling Enabled by Catalytic Generation of Chlorine Radicals. *J. Am. Chem. Soc.* **2016**, *138*, 12719–12722.
- (84) Li, P.; Deetz, A. M.; Hu, J.; Meyer, G. J.; Hu, K. Chloride Oxidation by One- or Two-Photon Excitation of N-Phenylphenothiazine. *J. Am. Chem. Soc.* **2022**, *144*, 17604–17610.
- (85) Rohe, S.; Morris, A. O.; McCallum, T.; Barriault, L. Hydrogen Atom Transfer Reactions via Photoredox Catalyzed Chlorine Atom Generation. *Angew. Chem., Int. Ed.* **2018**, *57*, 15664–15669.
- (86) Zidan, M.; Morris, A. O.; McCallum, T.; Barriault, L. The Alkylation and Reduction of Heteroarenes with Alcohols Using Photoredox Catalyzed Hydrogen Atom Transfer via Chlorine Atom Generation. *Eur. J. Org. Chem.* **2020**, 2020, 1453–1458.
- (87) Liu, L.; Fan, W.; Li, S. NaCl-Promoted Cobalt-Catalyzed Dioxygen-Mediated Methane Oxidation to Methylene Bis-(trifluoroacetate) with a Dramatic Salt Effect. ACS Catal. 2023, 13, 2396–2402.
- (88) Ermolenko, L. P.; Delaire, J. A.; Giannotti, C. Laser flash photolysis study of the mechanism of photooxidation of alkanes catalyzed by decatungstate anion. *J. Chem. Soc., Perkin Trans.* **1997**, *2*, 25–30.
- (89) McMillan, G.; Wijnen, M. H. J. Reactions of Alkoxy Radicals v. Photolysis of Di-t-butyl peroxide. *Can. J. Chem.* **1958**, *36*, 1227–1232.

- (90) Brook, J. H. T. Reaction of hydrocarbons with *tert.*-butoxy radicals. *Trans. Faraday Soc.* **1957**, *53*, 327–332.
- (91) Lunnak, S.; Sedlak, P. Photoinitiated reactions of hydrogen peroxide in the liquid phase. *J. Photochem. Photobiol., A* **1992**, *68*, 1–33
- (92) St. John, P. C.; Guan, Y.; Kim, Y.; Kim, S.; Paton, R. S. Prediction of organic homolytic bond dissociation enthalpies at near chemical accuracy with sub-second computational cost. *Nat. Commun.* **2020**, *11*, 2328.
- (93) Texier, I.; Delaire, J. A.; Giannotti, C. Reactivity of the charge transfer excited state of sodium decatungstate at the nanosecond time scale. *Phys. Chem. Chem. Phys.* **2000**, *2*, 1205–1212.
- (94) Wojnárovits, L.; Takács, E. Rate constants of dichloride radical anion reactions with molecules of environmental interest in aqueous solution: a review. *Environ. Sci. Pollut. Res.* **2021**, *28*, 41552–41575.
- (95) Lei, Y.; Lei, X.; Westerhoff, P.; Zhang, X.; Yang, X. Reactivity of Chlorine Radicals (Cl[•] and Cl₂[•]) with Dissolved Organic Matter and the Formation of Chlorinated Byproducts. *Environ. Sci. Technol.* **2021**, *55*, *689*–*699*.
- (96) Capaldo, L.; Ravelli, D. Decatungstate as Direct Hydrogen Atom Transfer Photocatalyst for SOMOphilic Alkynylation. *Org. Lett.* **2021**, 23, 2243–2247.
- (97) Tanielian, C. Decatungstate photocatalysis. *Coord. Chem. Rev.* **1998**, *178-180*, 1165–1181.
- (98) Hill, C. L. Introduction of functionality into unactivated carbon-hydrogen bonds Catalytic generation and nonconventional utilization of organic radicals. *Synlett* **1995**, *1995*, *127*–*132*.
- (99) Duncan, D. C.; Netzel, T. L.; Hill, C. L. Early-Time Dynamics and Reactivity of Polyoxometalate Excited States. Identification of a Short-Lived LMCT Excited State and a Reactive Long-Lived Charge-Transfer Intermediate following Picosecond Flash Excitation of $[W_{10}O_{32}]^{4-}$ in Acetonitrile. *Inorg. Chem.* **1995**, *34*, 4640–4646.
- (100) Ravelli, D.; Dondi, D.; Fagnoni, M.; Albini, A.; Bagno, A. Electronic and EPR spectra of the species involved in $[W_{10}O_{32}]^{4-}$ photocatalysis. A relativistic DFT investigation. *Phys. Chem. Chem. Phys.* **2013**, *15*, 2890–2896.
- (101) Duncan, D. C.; Fox, M. A. Early Events in Decatungstate Photocatalyzed Oxidations: A Nanosecond Laser Transient Absorbance Reinvestigation. *J. Phys. Chem. A* 1998, 102, 4559–4567.
- (102) Kothe, T.; Martschke, R.; Fischer, H. Photoreactions of the decatungstate anion $W_{10}O_{32}^{4-}$ with organic substrates in solution studied by EPR and kinetic absorption spectroscopy: an example for the persistent radical effect. *J. Chem. Soc., Perkin Trans.* **1998**, *2*, 503–508.
- (103) Tanielian, C.; Schweitzer, C.; Seghrouchni, R.; Esch, M.; Mechin, R. Polyoxometalate sensitization in mechanistic studies of photochemical reactions: The decatungstate anion as a reference sensitizer for photoinduced free radical oxygenations of organic compounds. *Photochem. Photobiol. Sci.* **2003**, *2*, 297–305.
- (104) Tanielian, C.; Seghrouchni, R.; Schweitzer, C. Decatungstate Photocatalyzed Electron-Transfer Reactions of Alkenes. Interception of the Geminate Radical Ion Pair by Oxygen. *J. Phys. Chem. A* **2003**, 107, 1102–1111.
- (105) Tanielian, C.; Lykakis, I. N.; Seghrouchni, R.; Cougnon, F.; Orfanopoulos, M. Mechanism of decatungstate photocatalyzed oxygenation of aromatic alcohols: Part I. Continuous photolysis and laser flash photolysis studies. *J. Mol. Catal. A: Chem.* **2007**, *262*, 170–175.
- (106) Tanielian, C.; Duffy, K.; Jones, A. Kinetic and Mechanistic Aspects of Photocatalysis by Polyoxotungstates: A Laser Flash Photolysis, Pulse Radiolysis, and Continuous Photolysis Study. *J. Phys. Chem. B* **1997**, *101*, 4276–4282.
- (107) Texier, I.; Delouis, J. F.; Delaire, J. A.; Giannotti, C.; Plaza, P.; Martin, M. M. Dynamics of the first excited state of the decatungstate anion studied by subpicosecond laser spectroscopy. *Chem. Phys. Lett.* **1999**, *311*, 139–145.
- (108) Chemseddine, A.; Sanchez, C.; Livage, J.; Launay, J. P.; Fournier, M. Electrochemical and photochemical reduction of decatungstate: a reinvestigation. *Inorg. Chem.* **1984**, 23, 2609–2613.

- (109) Armstrong, D. A.; Huie, R. E.; Koppenol, W. H.; Lymar, S. V.; Merényi, G.; Neta, P.; Ruscic, B.; Stanbury, D. M.; Steenken, S.; Wardman, P. Standard electrode potentials involving radicals in aqueous solution: inorganic radicals (IUPAC Technical Report). *Pure Appl. Chem.* **2015**, *87*, 1139–1150.
- (110) Ilyin, D. V.; Goddard, W. A.; Oppenheim, J. J.; Cheng, T. First-principles—based reaction kinetics from reactive molecular dynamics simulations: Application to hydrogen peroxide decomposition. *Proc. Natl. Acad. Scic. USA* **2019**, *116*, 18202—18208.
- (111) Kundu, S.; Zanganeh, J.; Moghtaderi, B. A review on understanding explosions from methane—air mixture. *J. Loss Prev. Process Ind.* **2016**, *40*, 507–523.
- (112) Protti, S.; Ravelli, D.; Fagnoni, M.; Albini, A. Solar light-driven photocatalyzed alkylations. Chemistry on the window ledge. *Chem. Commun.* **2009**, 7351–7353.

☐ Recommended by ACS

Carbene Radicals in Transition-Metal-Catalyzed Reactions

Roel F.J. Epping, Bas de Bruin, et al.

APRIL 06, 2023 ACS CATALYSIS

READ 🗹

Extending Photocatalyst Activity through Choice of Electron Donor

Felicity Draper, Timothy U. Connell, et al.

JANUARY 11, 2023

THE JOURNAL OF ORGANIC CHEMISTRY

READ 🗹

Explaining Kinetic Trends of Inner-Sphere Transition-Metal-Ion Redox Reactions on Metal Electrodes

Harsh Agarwal, Nirala Singh, et al.

JANUARY 27, 2023

ACS CATALYSIS

READ 🗹

Silica Supported Organometallic Ir¹ Complexes Enable Efficient Catalytic Methane Borylation

Orion Staples, Daniel J. Mindiola, et al.

MARCH 30, 2023

JOURNAL OF THE AMERICAN CHEMICAL SOCIETY

READ 🗹

Get More Suggestions >